CivilEng

MDPI

Article

Optimizing the Location of Supports under a Monolithic Floor Slab

Anton Chepurnenko [1,*], Vasilina Turina [1] and Vladimir Akopyan [2]

[1] Structural Mechanics and Theory of Structures Department, Don State Technical University, 344003 Rostov-on-Don, Russia; vasilina.93@mail.ru
[2] Engineering Geology, Bases and Foundations Department, Don State Technical University, 344003 Rostov-on-Don, Russia; vovaakop@mail.ru
* Correspondence: anton_chepurnenk@mail.ru

Abstract: Monolithic reinforced concrete floor slabs are one of the most common types of building structures, and their optimization is an urgent task. The article presents the methodology for finding the optimal position of point supports under a reinforced concrete floor slab of arbitrary configuration at arbitrary load. The slab is considered thin, elastic and isotropic, with constant over-the-area stiffness, that is, the reinforcement is not taken into account or is constant. The solution is performed using the finite element method in combination with the nonlinear optimization methods. Finite element analysis is implemented by authors in MATLAB (R2024a) environment in such a way that the location of the columns may not coincide with the nodes of the finite element mesh of the slab. This allows to significantly increase the efficiency of solving the optimization problem compared to previously used algorithms, including the Monte Carlo method. Boundary conditions are taken into account using the Lagrange multiplier method. As an optimization criterion, the maximum deflection value is used, as well as the value of the potential strain energy. The effectiveness of six nonlinear optimization methods is compared in the example of a square slab under the action of a uniformly distributed load. For solutions obtained using the pattern search, simulated annealing and internal point methods, the maximum deflections are at least 1.2 times higher than for solutions obtained using the particle swarm method and genetic algorithm. An example of real object optimization is also presented. By changing the position of seven columns, it was possible to reduce the maximum deflection of the floor slab by 1.6 times.

Keywords: finite element method; optimization; reinforced concrete; monolithic floor slab; genetic algorithm; particle swarm method

Citation: Chepurnenko, A.; Turina, V.; Akopyan, V. Optimizing the Location of Supports under a Monolithic Floor Slab. *CivilEng* **2024**, *5*, 502–520. https://doi.org/10.3390/civileng5020026

Academic Editors: Angelo Luongo and Francesco D'Annibale

Received: 13 March 2024
Revised: 13 May 2024
Accepted: 13 June 2024
Published: 14 June 2024

1. Introduction

The issues of the optimal design of reinforced concrete structures are the subject of research by many scientists. One of the most common ways to optimize reinforced concrete structures, including monolithic reinforced concrete slabs, is the selection of rational reinforcement [1–7] and the rational installation of ribs [8,9]. In addition to varying the reinforcement coefficient, another way to optimize slab structures can be to vary their thickness [10], due to which the structure becomes of equal strength. An equal strength state can also be achieved by varying the physical and mechanical characteristics of the material by volume [11–15]. The practical implementation of the last two methods is associated with significant difficulties. Floor slabs of variable thickness are currently practically not used in construction due to the complexity of their manufacturing technology. Vibrocentrifuged columns are an example of structures with mechanical characteristics that vary in volume [16–20]. In such structures, the modulus of elasticity of concrete and its strength are the functions of the radius. Radial heterogeneity is created when the hardening material rotates due to inertial forces. For slabs, it is not possible to create artificial heterogeneity in this way.

The efficient use of material in cast in situ reinforced concrete slabs can also be achieved by the rational installation of supports [21,22]. Currently, in the literature, optimization problems by varying the position of supports are presented mainly for beams [23–26]. Works in which slabs are the object of study contain solutions to fairly simple problems. In [27], for example, the case of an annular plate under an axisymmetric load is considered. Papers [28–33] present a solution for a square slab with four point supports.

When solving problems of finding the optimal supports location, various optimization criteria are used. Quite often, the frequency of the natural vibrations of the structure acts as a criterion. The article [34] proposes a technique for maximizing the first vibration frequency of building structures based on the topological optimization method. The supports function as elastic springs. Test examples are given for some beams, slabs and shells. The issue of finding the optimal distribution of elastic springs for structures that experience vibrations is also considered in [35] using the example of cantilever beams on an elastic foundation. The article [36] searches for the optimal location of viscoelastic supports for the effective damping of beam vibrations under harmonic excitation.

The magnitude of internal forces is also widely used as an optimization criterion. In the work [37], the location of supports under the bridge in the form of a multi-span beam is optimized from the condition of the equality of the maximum bending moments in the span and on the supports.

In [38], when optimizing the position of supports under multi-span beams, the criterion is the maximum deflection. In the article [39], the L^2 norm of the structure displacements is used as an optimization criterion, which, in comparison with the maximum deflection, is a more integral characteristic that reflects the operation of the structure. Optimization examples of beams and plates subjected to their own weight are considered in the mentioned publication.

Potential strain energy can also serve as an integral measure characterizing the efficiency of a structure [40]. The paper [41] shows that the arrangement of supports in monolithic reinforced concrete slabs, which satisfies the minimum potential strain energy, also corresponds to the minimum consumption of reinforcement. The optimization technique presented in [42] allows for optimizing only rectangular slabs with a regular arrangement of columns, varying only the column spacing along the x- and y-axes.

In paper [21], an algorithm was proposed for finding the optimal location of supports under monolithic floor slabs with an arbitrary shape, based on the Monte Carlo method. The essence of this algorithm was that n columns were randomly located at the nodes of the finite element mesh, and a finite element calculation was carried out repeatedly with a random arrangement of columns. The best one was chosen from many options, and with a large number of tests, this result approached the optimal one. This approach worked well with a small number of supports (no more than 6); but with an increase in the number of supports, its effectiveness decreased significantly.

The purpose of this work is to develop a more effective technique for finding the optimal position of point supports under a monolithic reinforced concrete slab. The developed methodology must be applicable for the arbitrary configuration of the slab and arbitrary loads. Based on the experience of previous studies, two optimization criteria will be used: the maximum deflection of the slab $w_{\max}$ and the potential strain energy W. The optimal design solution will correspond to the minimum of the objective function, which is the value $w_{\max}$ or W. In the present study, the slabs are assumed to be thin, isotropic and elastic. The fact that the slab is thin implies that transverse shear deformations are not taken into account. Slab reinforcement is also not taken into account when solving the optimization problem. The justification for the assumptions made will be given further in the next section.

2. Materials and Methods

The optimization technique will be considered using the example of a square slab supported by n columns and subjected to a load uniformly distributed over the area. The floor slab is considered beamless, that is, it is supported only by columns.

The optimization problem is solved using the finite element method (FEM) in combination with the nonlinear optimization methods embedded in the Optimization Toolbox and Global Optimization Toolbox packages of the MATLAB environment. The following nonlinear optimization methods are used:

1. Interior point method;
2. Genetic algorithm;
3. Pattern search method;
4. Surrogate optimization method;
5. Particle swarm method;
6. Simulated annealing method.

The slab, depending on the geometry, is meshed by rectangular (Figure 1) or triangular (Figure 2) finite elements (FEs) with three degrees of freedom at the node: deflection w_i and rotation angles φ_i^x and φ_i^y. Columns are treated as point restraints in z direction. Punching effects are not considered when solving an optimization problem.

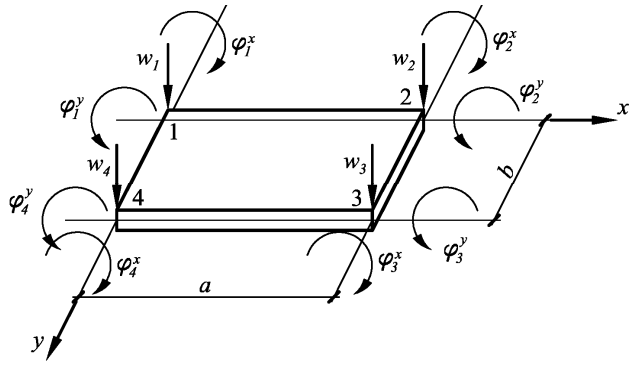

Figure 1. Rectangular slab finite element.

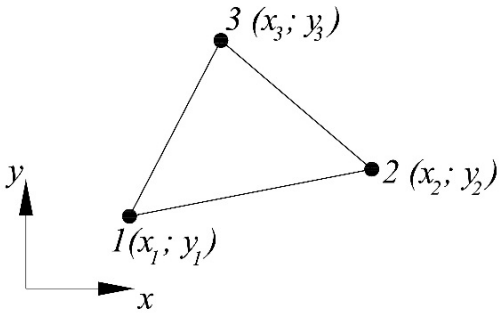

Figure 2. Triangular slab finite element.

The variable input parameters of the objective function are the x and y coordinates of each column. Thus, if there are n columns, the position of which can change, the total number of input parameters of the objective function is $2n$.

To prevent the need to re-generate the FE mesh during the optimization process when changing the position of the supports, the finite element analysis is implemented in such a way that the location of the columns may not coincide with the mesh nodes. This allows us to significantly save machine time during the optimization process.

At the first stage, the stiffness matrix of the slab is formed without taking into account the columns, the location of which can change. By default, the MATLAB environment does not allow for calculating slabs subjected to bending using the FEM. The objective

function is written in the MATLAB programming language which implements the FEM. In the process of the solution, each time the objective function is called, the corresponding boundary conditions are imposed for the x and y coordinates of each column. The method of Lagrange multipliers is used to take into account the boundary conditions.

The process of boundary condition imposition will be considered at first on the example of a rectangular finite element. The deflection for a rectangular FE is approximated by the following function:

$$\begin{array}{l} w = f_1 + f_2 x + f_3 y + f_4 x^2 + f_5 y^2 + f_6 xy + f_7 x^2 y + \\ + f_8 xy^2 + f_9 x^3 + f_{10} y^3 + f_{11} x^3 y + f_{12} xy^3. \end{array} \tag{1}$$

The rotation angles can be found by differentiating expression (1). The expressions for deflections and rotation angles will take the following form:

$$\begin{array}{c} \left\{ w \quad \frac{\partial w}{\partial x} \quad \frac{\partial w}{\partial y} \right\}^{\mathrm{T}} \\ = \begin{bmatrix} 1 & x & y & x^2 & y^2 & xy & x^2 y & xy^2 & x^3 & y^3 & x^3 y & xy^3 \\ 0 & 1 & 0 & 2x & 0 & y & 2xy & y^2 & 3x^2 & 0 & 3x^2 y & y^3 \\ 0 & 0 & 1 & 0 & 2y & x & x^2 & 2xy & 0 & 3y^2 & x^3 & 3y^2 x \end{bmatrix} \{f\}, \end{array} \tag{2}$$

where $\{f\}^{\mathrm{T}} = \{f_1\ f_2\ f_3\ f_4\ f_5\ f_6\ f_7\ f_8\ f_9\ f_{10}\ f_{11}\ f_{12}\}$.

In Figure 1: $\varphi_i^x = \frac{\partial w_i}{\partial x}; \varphi_i^y = \frac{\partial w_i}{\partial y}$.

Substituting the coordinates of the nodes of the finite element into (2), the following equality can be obtained:

$$\{U^e\} = [C] \cdot \{f\} \tag{3}$$

where $\{U^e\} = \left\{ \begin{array}{cccccccccccc} w_1 & \varphi_1^x & \varphi_1^y & w_2 & \varphi_2^x & \varphi_2^y & w_3 & \varphi_3^x & \varphi_3^y & w_4 & \varphi_4^x & \varphi_4^y \end{array} \right\}^T$ is the element nodal displacement vector,

$$[C] = \begin{bmatrix} 1 & 0 & 0 & 0 & 0 & 0 & 0 & 0 & 0 & 0 & 0 & 0 \\ 0 & 1 & 0 & 0 & 0 & 0 & 0 & 0 & 0 & 0 & 0 & 0 \\ 0 & 0 & 1 & 0 & 0 & 0 & 0 & 0 & 0 & 0 & 0 & 0 \\ 1 & a & 0 & a^2 & 0 & 0 & 0 & 0 & a^3 & 0 & 0 & 0 \\ 0 & 1 & 0 & 2a & 0 & 0 & 0 & 0 & 3a^2 & 0 & 0 & 0 \\ 0 & 0 & 1 & 0 & 0 & a & a^2 & 0 & 0 & 0 & a^3 & 0 \\ 1 & a & b & a^2 & b^2 & ab & a^2 b & ab^2 & a^3 & b^3 & a^3 b & ab^3 \\ 0 & 1 & 0 & 2a & 0 & b & 2ab & b^2 & 3a^2 & 0 & 3a^2 b & b^3 \\ 0 & 0 & 1 & 0 & 2b & a & a^2 & 2ab & 0 & 3b^2 & a^3 & 3ab^2 \\ 1 & 0 & b & 0 & b^2 & 0 & 0 & 0 & 0 & b^3 & 0 & 0 \\ 0 & 1 & 0 & 0 & 0 & b & 0 & b^2 & 0 & 0 & 0 & b^3 \\ 0 & 0 & 1 & 0 & 2b & 0 & 0 & 0 & 0 & 3b^2 & 0 & 0 \end{bmatrix}. \tag{4}$$

From (3), it follows that $\{f\} = [C]^{-1} \cdot \{U^e\}$.

If a point with coordinates $(x_0; y_0)$ is fixed along the z axis, then, taking into account (1), for this point, it can be written as follows:

$$\begin{array}{c} w(x_0, y_0) = 0 \rightarrow \\ \rightarrow \left[\begin{array}{cccccccccccc} 1 & x_0 & y_0 & x_0^2 & y_0^2 & x_0 y_0 & x_0^2 y_0 & x_0 y_0^2 & x_0^3 & y_0^3 & x_0^3 y_0 & x_0 y_0^3 \end{array} \right] \{f\} = 0, \end{array} \tag{5}$$

or

$$\left[\begin{array}{cccccccccccc} 1 & x_0 & y_0 & x_0^2 & y_0^2 & x_0 y_0 & x_0^2 y_0 & x_0 y_0^2 & x_0^3 & y_0^3 & x_0^3 y_0 & x_0 y_0^3 \end{array} \right] [C]^{-1} \{U^e\} = 0. \tag{6}$$

For n columns, n conditions are obtained, which can be represented as

$$[B]\{U\} = 0, \tag{7}$$

where $[B]$ is a matrix of size $n \cdot (3 \cdot np)$ (np is the total number of nodes) and $\{U\}$ is the vector of the nodal displacements of the entire slab.

For a triangular element, the deflection function is approximated by a polynomial with nine uncertain coefficients $\beta_{1\ldots9}$ in accordance with the total number of FE bending degrees of freedom:

$$w = \beta_1 L_1 + \beta_2 L_2 + \beta_3 L_3 + \beta_4 \left(L_2^2 L_1 + \frac{1}{2} L_1 L_2 L_3 \right) + \ldots + \beta_9 \left(L_1^2 L_3 + \frac{1}{2} L_1 L_2 L_3 \right). \quad (8)$$

$L_1,\ L_2,\ L_3$ here are the natural coordinates, which are defined as follows:

$$L_i = \frac{1}{2A}(a_i + b_i x + c_i y), i = 1 \ldots 3, \quad (9)$$

where $A = \frac{1}{2} \begin{vmatrix} 1 & x_1 & y_1 \\ 1 & x_2 & y_2 \\ 1 & x_3 & y_3 \end{vmatrix}$ is the area of the triangular FE, $a_1 = x_2 y_3 - x_3 y_2$, $b_1 = y_2 - y_3$, $c_1 = x_3 - x_2$.

The coefficients a_i, b_i, c_i for $i = 2$ and $i = 3$ are determined by cyclically replacing the indices $1 \to 2 \to 3 \to 1$.

Such an approximation for a triangular FE is proposed in [42]. Coefficients β_j with j in $\{1\ldots9\}$ can be found by substituting the nodal values of deflections and rotation angles into expression (8). To obtain expressions for the rotation angles φ_x and φ_y, the deflection function must be differentiated with respect to x and y, respectively. Differentiation by Cartesian coordinates is performed as follows:

$$\begin{aligned} \frac{\partial}{\partial x} &= \frac{\partial L_1}{\partial x}\frac{\partial}{\partial L_1} + \frac{\partial L_2}{\partial x}\frac{\partial}{\partial L_2} + \frac{\partial L_3}{\partial x}\frac{\partial}{\partial L_3} = \frac{1}{2A}\left(b_1 \frac{\partial}{\partial L_1} + b_2 \frac{\partial}{\partial L_2} + b_3 \frac{\partial}{\partial L_3} \right); \\ \frac{\partial}{\partial y} &= \frac{\partial L_1}{\partial y}\frac{\partial}{\partial L_1} + \frac{\partial L_2}{\partial y}\frac{\partial}{\partial L_2} + \frac{\partial L_3}{\partial y}\frac{\partial}{\partial L_3} = \frac{1}{2A}\left(c_1 \frac{\partial}{\partial L_1} + c_2 \frac{\partial}{\partial L_2} + c_3 \frac{\partial}{\partial L_3} \right). \end{aligned} \quad (10)$$

After determining the coefficients $\beta_{1..9}$, the function w is expressed in terms of the nodal displacements of the element as follows:

$$w = \{ \ \{N_1\} \quad \{N_2\} \quad \{N_3\} \ \} \{U^e\} = \{\Psi\}\{U^e\}, \quad (11)$$

where $\{N_1\},\ \{N_2\},\ \{N_3\}$ are the shape functions.

$$\{N_1\}^T = \begin{Bmatrix} L_1 + L_1^2 L_2 + L_1^2 L_3 - L_1 L_2^2 - L_1 L_3^2 \\ b_3 \left(L_1^2 L_2 + \frac{1}{2} L_1 L_2 L_3 \right) - b_2 \left(L_3 L_1^2 + \frac{1}{2} L_1 L_2 L_3 \right) \\ c_3 \left(L_1^2 L_2 + \frac{1}{2} L_1 L_2 L_3 \right) - c_2 \left(L_3 L_1^2 + \frac{1}{2} L_1 L_2 L_3 \right) \end{Bmatrix}. \quad (12)$$

To obtain expressions for $\{N_2\}$ and $\{N_3\}$, a cyclic substitution of indices is performed in formula (12).

For a point with coordinates x_0 and y_0, at which the column is located, it can be written as follows:

$$\{\Psi(x_0, y_0)\}\{U^e\} = 0. \quad (13)$$

By writing condition (13) for n point supports, the expression in the form (7) can be obtained.

The system of FEM equations, taking into account the boundary conditions (7) when using the Lagrange multiplier method, has the following form [43]:

$$\begin{bmatrix} [K] & [B]^T \\ [B] & 0 \end{bmatrix} \begin{Bmatrix} \{U\} \\ \{\lambda\} \end{Bmatrix} = \begin{Bmatrix} \{F\} \\ 0 \end{Bmatrix}, \quad (14)$$

where $[K]$ is the stiffness matrix of the slab without taking into account the supports, the position of which can change, $\{\lambda\}$ is the vector of Lagrange multipliers, and $\{F\}$ is the vector of nodal loads.

Due to the fact that the structure stiffness matrix is generated only once taking into account only stationary columns, significant savings in machine time are achieved.

After finding the vector of nodal displacements $\{U\}$ by solving the system of Equation (14), the potential strain energy (PSE) of the slab is calculated by the following formula:

$$W = \frac{1}{2}\{U\}^T[K]\{U\}. \quad (15)$$

The flowchart of the optimization process is shown in Figure 3.

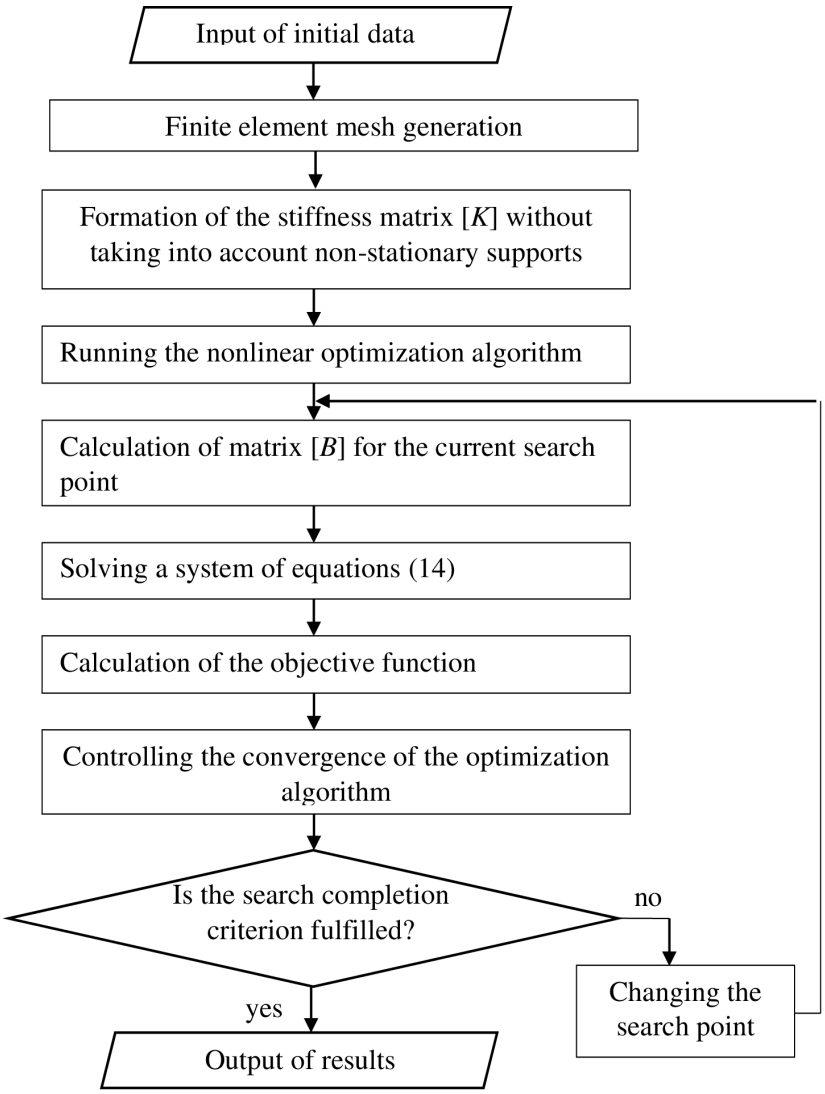

Figure 3. Flowchart of the optimization process.

The stiffness matrix $[K]$ in this study is calculated as for a thin isotropic slab without taking into account transverse shear deformations, physical nonlinearity and reinforcement. Transverse shear deformations are not taken into account since thin slabs are considered, in which the thickness-to-span ratio does not exceed $\frac{1}{5}$. Ignoring physical nonlinearity is justified by the fact that finite element calculations in a physically nonlinear formulation require much more computer time compared to linear calculations. During the optimization process, this calculation must be repeated many times. Depending on the number of input

parameters of the target function, the number of iterations in the optimization process can reach hundreds or more. In the case of a physically nonlinear analysis, each iteration will include many subiterations. In addition, most structures under operational loads are characterized by work close to the elastic range. Noticeable nonlinearity appears only under extreme influences. We also assume that a structure that performs optimally in the elastic stage will also perform well beyond elasticity.

As for reinforcement, in the case of constant reinforcement on the entire area of the slab, it can be taken into account by increasing the flexural stiffness of the slab. Moreover, as has been shown in [21], the optimal location of the supports does not depend on the stiffness of the slab if it is constant over the slab entire area. Quite often, monolithic floor slabs have variable reinforcement with an increase in areas with the highest bending moments. When the position of the supports changes, the maximum bending moments are redistributed. Considering this factor is as complicated as taking into account physical nonlinearity and requires recalculating the slab stiffness matrix at each iteration.

It should also be noted that, as a rule, in calculation software such as CivilFEM 2022, Lira-SAPR 2024, SCAD 11.7, etc., the selection of reinforcement is carried out according to internal forces determined in elastic isotropic structure without reinforcement, since it is not known in advance how much reinforcement is required.

The cross-sectional dimensions of the column are not taken into account, since this will affect the stress pattern in the immediate vicinity of the column, but not the performance of the slab as a whole. Taking into account the cross-sectional dimensions of the column will have virtually no effect on the maximum deflections of the slab.

3. Results and Discussion

At the first stage, the optimization technique was tested on a square slab 10 × 10 m in size, 0.2 m thick, subjected to the load q = 20 kN/m^2 uniformly distributed over the area. The modulus of the elasticity of concrete was $E = 3.25 \times 10^4$ MPa and the Poisson's ratio was $\nu = 0.2$. The number of columns varied from 3 to 10. The slab was meshed by square finite elements. To select the optimal size of the finite element mesh, a calculation was performed with the finite element rib size equal to 1 m, 0.5 m, 0.25 m. It was found that with mesh sizes of 0.5 m and 0.25 m, the value of the maximum deflection and potential strain energy practically do not change. The final value of the FE rib size was taken to be 0.5 m.

To narrow the search area and speed up the solution of the problem, the slab was divided by x into n segments $\Delta x = L/n$, where L is the size of the slab in plan; and for the i-th column, the search area was limited to the i-th segment and two neighboring ones. Constraints on the x coordinate for the i-th column can be represented as follows:

$$\begin{gathered}(i-2)\cdot\Delta x \le x_i \le (i+1)\cdot\Delta x,\ i = 2\ldots n-1;\\ 0 \le x_1 \le 2\Delta x;\\ L - 2\Delta x \le x_n \le L.\end{gathered} \tag{16}$$

The y coordinate for all columns ranged from 0 to L.

Table 1 presents the results of solving the optimization problem by various methods. Bold indicates the best results for each n. The criterion for the efficiency of optimization algorithms was the minimum value of the objective function at the output. For $n > 3$, the surrogate optimization, pattern search, interior point, and simulated annealing methods showed lower efficiency, and therefore, the results are not shown in Table 1. The lower efficiency of the interior point, pattern search, and simulated annealing methods can be explained by the fact that these methods require setting the initial search point. In the problem under consideration, there are many local minima, which are not always global and lead to the termination of the algorithm. As an illustration, Figure 4 shows the progress of the optimization process at n = 5 in the case of optimization according to the criterion of minimum deflection.

Table 1. Results of solving the optimization problem.

Number of Columns n	Algorithm	Optimization Criterion	w_{max}, mm	W, kJ
3	Surrogate optimization	Minimum deflection	31.9	13.8464
3	Surrogate optimization	Minimum PSE	45.5	9.14
3	Pattern search	Minimum deflection	49.1	18.3690
3	Pattern search	Minimum PSE	43.6	8.9258
3	Interior point	Minimum deflection	36.1	10.6883
3	Interior point	Minimum PSE	43.6	8.9258
3	Simulated annealing	Minimum deflection	44.4	9.9807
3	Simulated annealing	Minimum PSE	45.3	8.9176
3	Genetic	Minimum deflection	31.8	13.1231
3	Genetic	Minimum PSE	47.4	**8.9093**
3	Particle swarm	Minimum deflection	**30.1**	11.8760
3	Particle swarm	Minimum PSE	47.4	**8.9093**
4	Genetic	Minimum deflection	**5.12**	2.7803
4	Genetic	Minimum PSE	5.25	**2.6488**
4	Particle swarm	Minimum deflection	5.64	3.0189
4	Particle swarm	Minimum PSE	5.25	**2.6488**
5	Genetic	Minimum deflection	4.5	2.1360
5	Genetic	Minimum PSE	5.15	2.0399
5	Particle swarm	Minimum deflection	**4.44**	2.3249
5	Particle swarm	Minimum PSE	5.36	**2.0366**
6	Genetic	Minimum deflection	3.89	1.9124
6	Genetic	Minimum PSE	5.8578	1.4440
6	Particle swarm	Minimum deflection	**3.35**	1.6955
6	Particle swarm	Minimum PSE	4.6	**1.4344**
7	Genetic	Minimum deflection	5.15	2.3305
7	Genetic	Minimum PSE	4.23	1.0243
7	Particle swarm	Minimum deflection	**2.95**	1.3748
7	Particle swarm	Minimum PSE	4.19	**1.0227**
8	Genetic	Minimum deflection	2.47	1.1119
8	Genetic	Minimum PSE	4.35	0.7327
8	Particle swarm	Minimum deflection	**2.17**	1.1563
8	Particle swarm	Minimum PSE	2.58	**0.7115**
9	Genetic	Minimum deflection	1.71	0.7663
9	Genetic	Minimum PSE	**1.0621**	**0.4888**
9	Particle swarm	Minimum deflection	1.71	0.9135
9	Particle swarm	Minimum PSE	2.39	0.6316
10	Genetic	Minimum deflection	1.78	0.8878
10	Genetic	Minimum PSE	1.56	0.4288
10	Particle swarm	Minimum deflection	1.25	0.6776
10	Particle swarm	Minimum PSE	**1.04**	**0.4137**

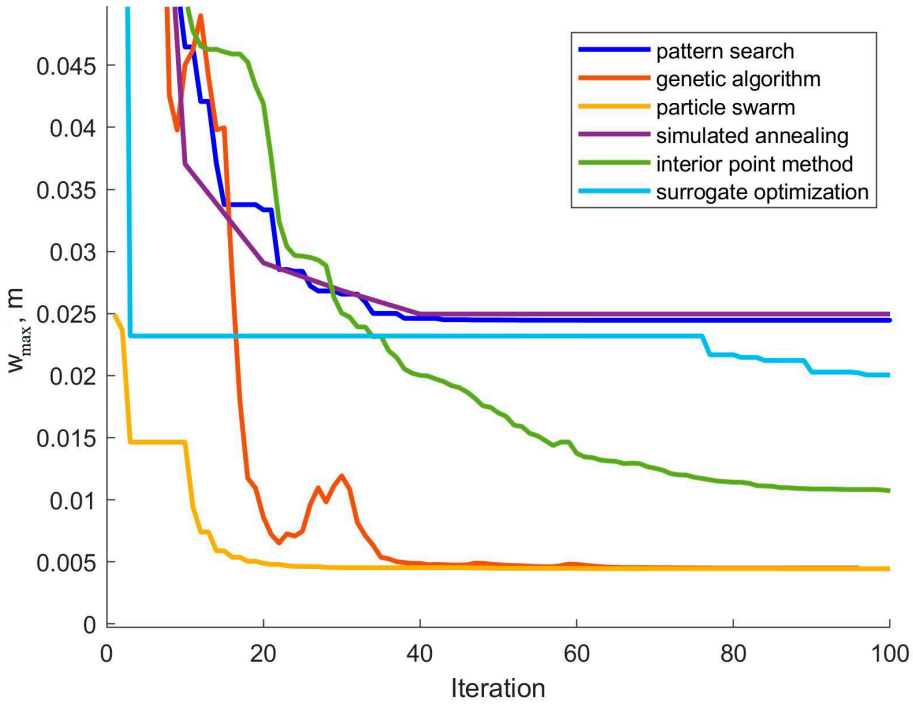

Figure 4. Convergence plot at $n = 5$ when using the criterion of minimum deflection.

The genetic algorithm and the particle swarm method showed approximately the same efficiency. For some n, the best solution was obtained by the first method, and for others by the second. At $n = 4$, in the case of using the criterion of the minimum PSE, the results obtained by the two methods are the same. Comparing the performance of these two methods is the subject of many studies, including [44–47], etc. Our study confirms the conclusions about the approximately equal efficiency of the genetic algorithm and the particle swarm method made in [44–47]. Some authors use these methods in combination [48–52].

Figures 5–12 show the obtained optimal positions of the columns for various n, as well as the isofields of vertical displacements. The columns are marked with red markers. The color scale shows vertical displacements in meters. At $n = 3, 4$, the solutions are consistent with those given in [21,30,31,33,53]. It is noteworthy that the solutions based on the criterion of the minimum PSE are close to the solutions based on the criterion of the maximum first natural frequency. For example, with $n = 4$, the optimal ratio of a/L (Figure 13) from the condition of the maximum of the first frequency is 0.2–0.3, and from the condition of the minimum potential strain energy, it is 0.227. The calculation of the first natural frequency is more expensive in terms of computer time, since it requires solving the problem of eigenvalues instead of solving a system of linear algebraic equations. Therefore, in our opinion, the use of the criterion of minimum potential strain energy is preferable.

It should also be noted that the solutions obtained on the basis of the minimum PSE criterion are characterized by greater symmetry and regularity. This is due to the fact that deflection is a local characteristic of the structure, which can change significantly with a slight change in the position of individual columns. Potential strain energy, on the contrary, is an integral characteristic of the structure, showing the efficiency of its operation as a whole. For large n, the search for the optimal solution according to the minimum PSE criterion also leads to the minimum deflection, as can be seen from Table 1 for $n = 9, 10$.

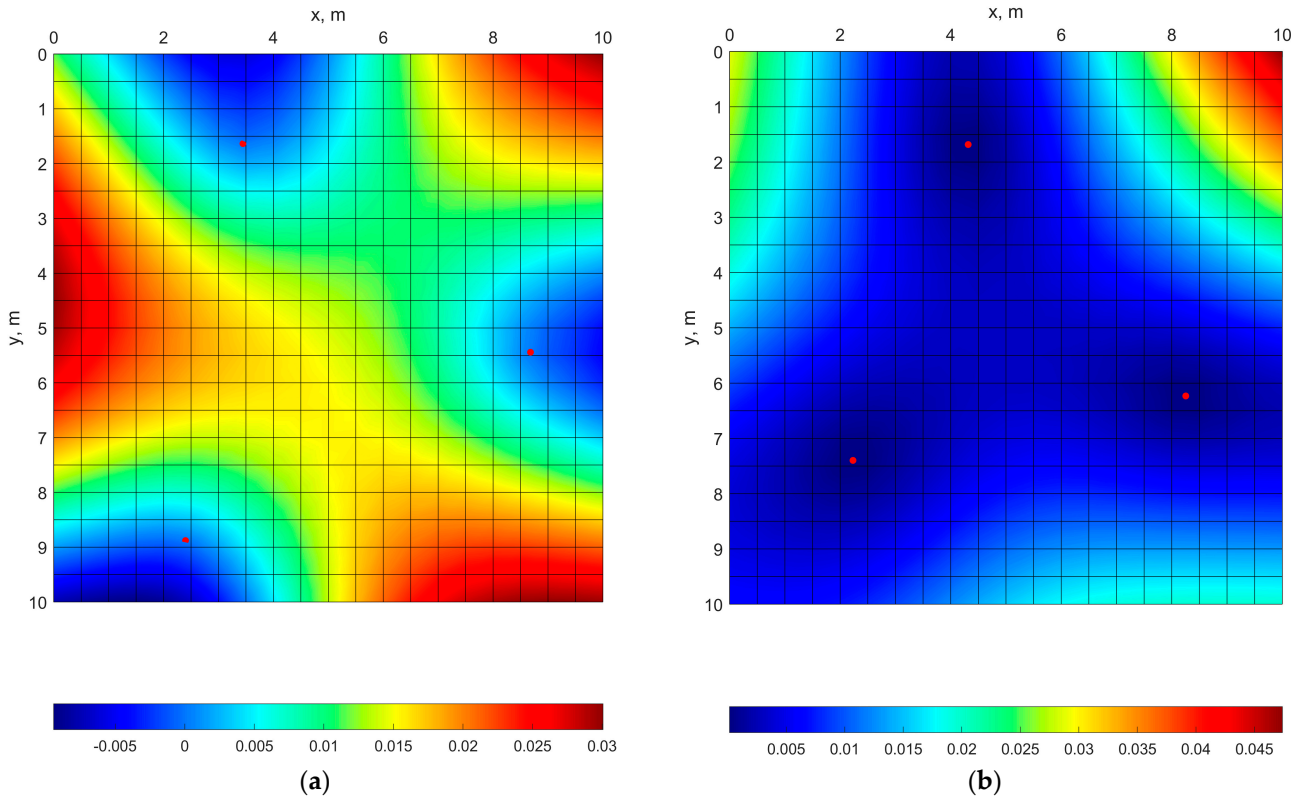

(**a**) (**b**)

Figure 5. Optimal location of the columns and isofields of vertical displacements (m) at $n = 3$: (**a**) from the minimum deflection condition; (**b**) from the PSE minimum condition.

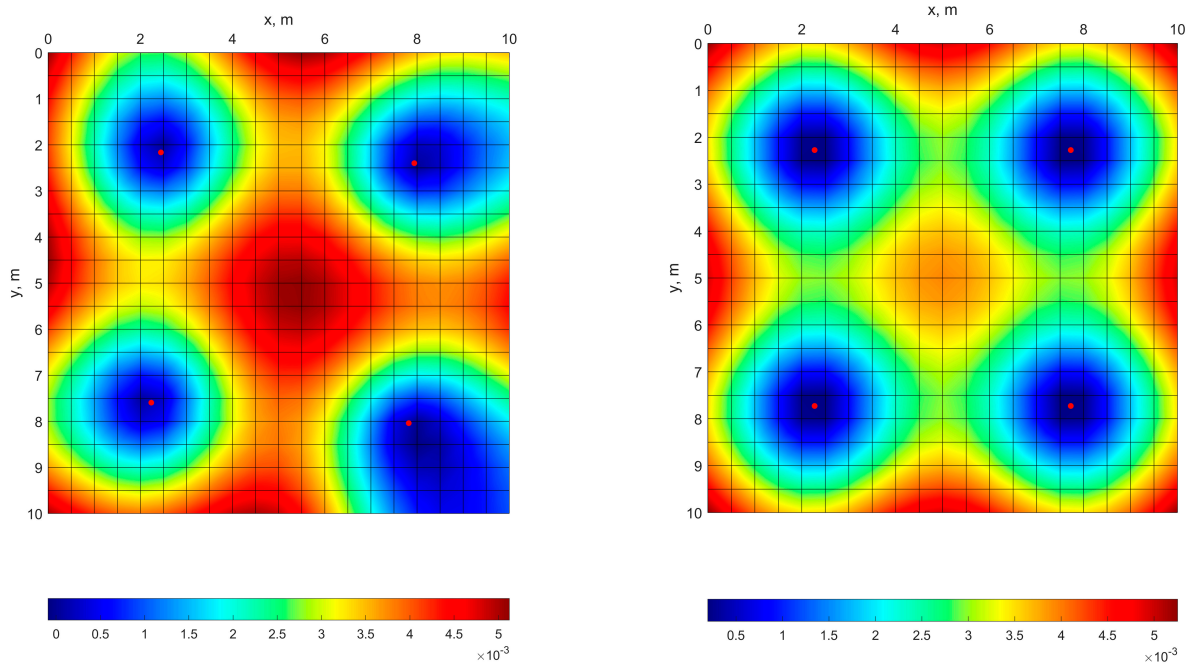

(**a**) (**b**)

Figure 6. Optimal location of the columns and isofields of vertical displacements (m) at $n = 4$: (**a**) from the minimum deflection condition; (**b**) from the PSE minimum condition.

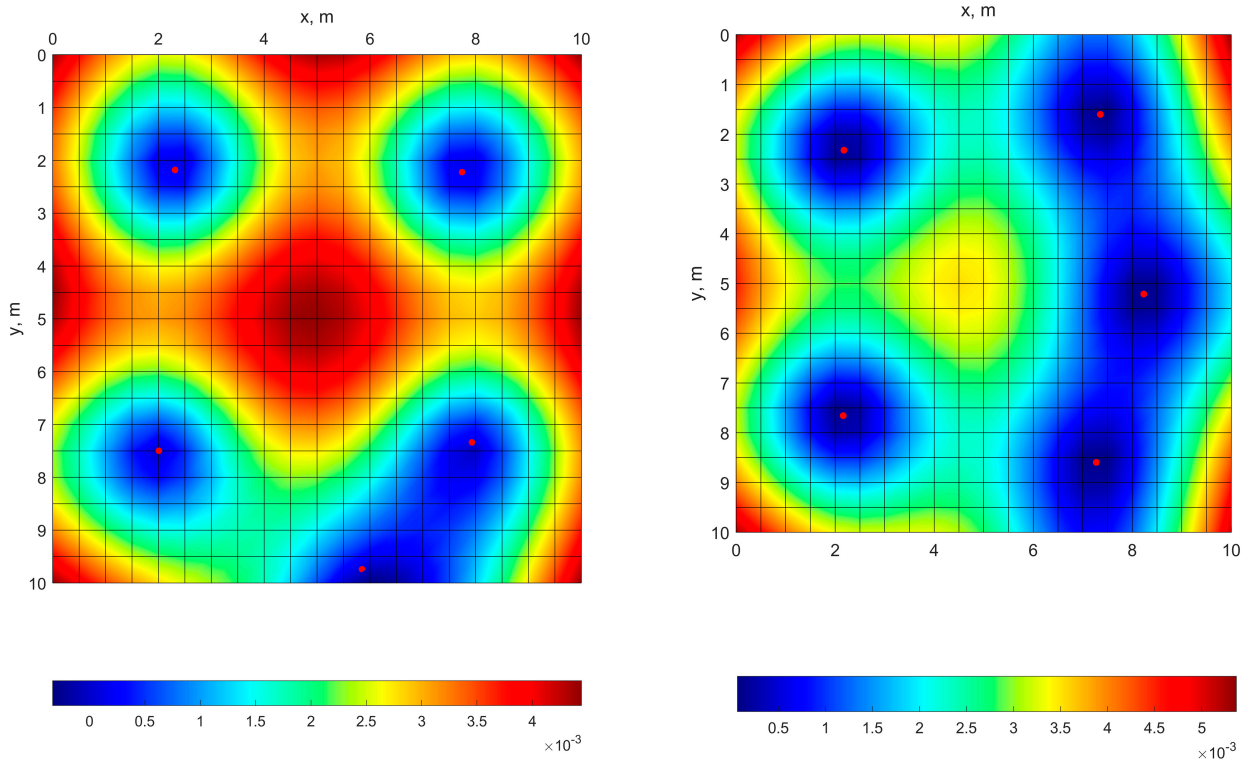

(**a**) (**b**)

Figure 7. Optimal location of the columns and isofields of vertical displacements (m) at $n = 5$: (**a**) from the minimum deflection condition; (**b**) from the PSE minimum condition.

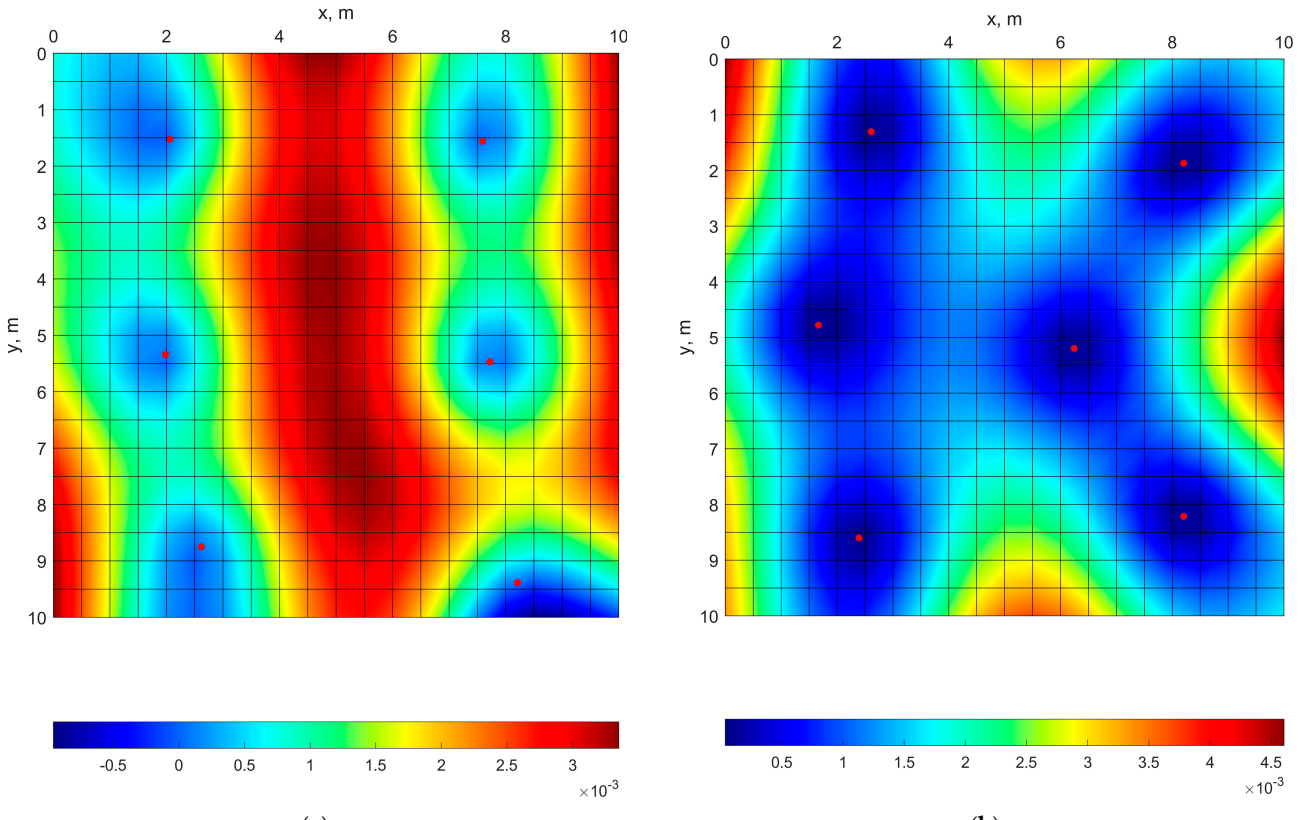

(**a**) (**b**)

Figure 8. Optimal location of the columns and isofields of vertical displacements (m) at $n = 6$: (**a**) from the minimum deflection condition; (**b**) from the PSE minimum condition.

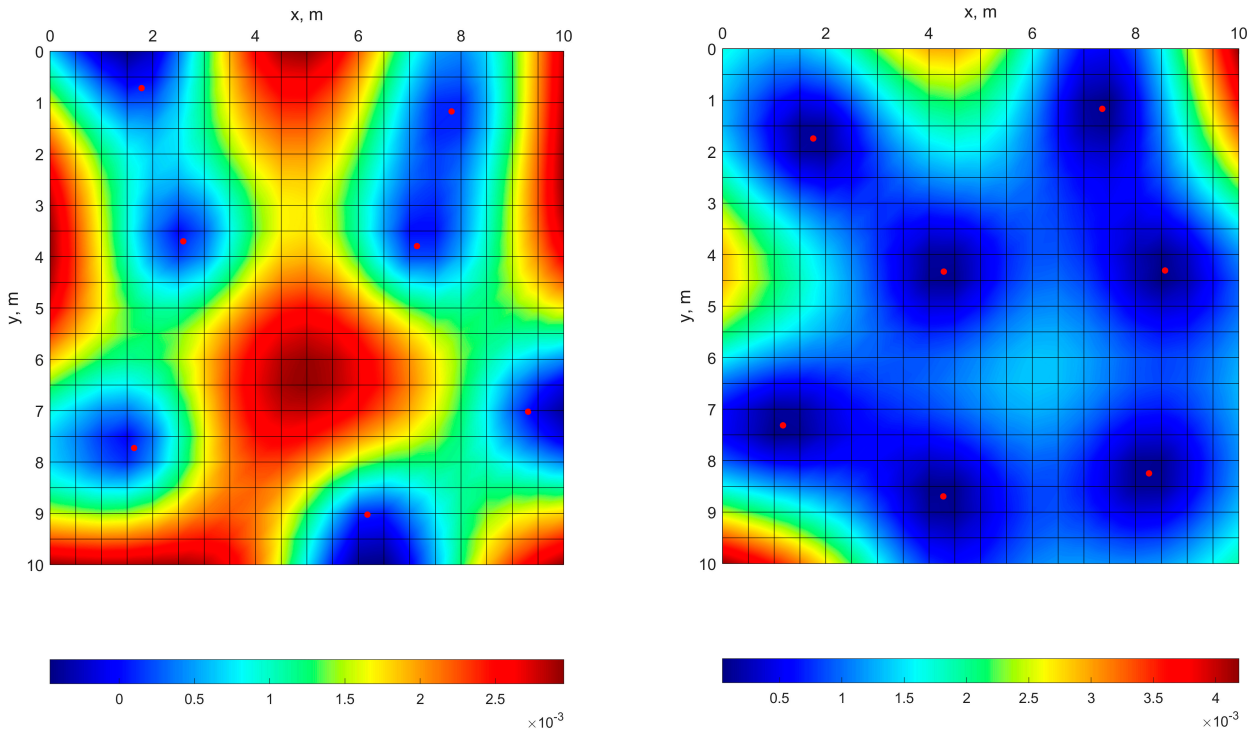

(**a**) (**b**)

Figure 9. Optimal location of the columns and isofields of vertical displacements (m) at $n = 7$: (**a**) from the minimum deflection condition; (**b**) from the PSE minimum condition.

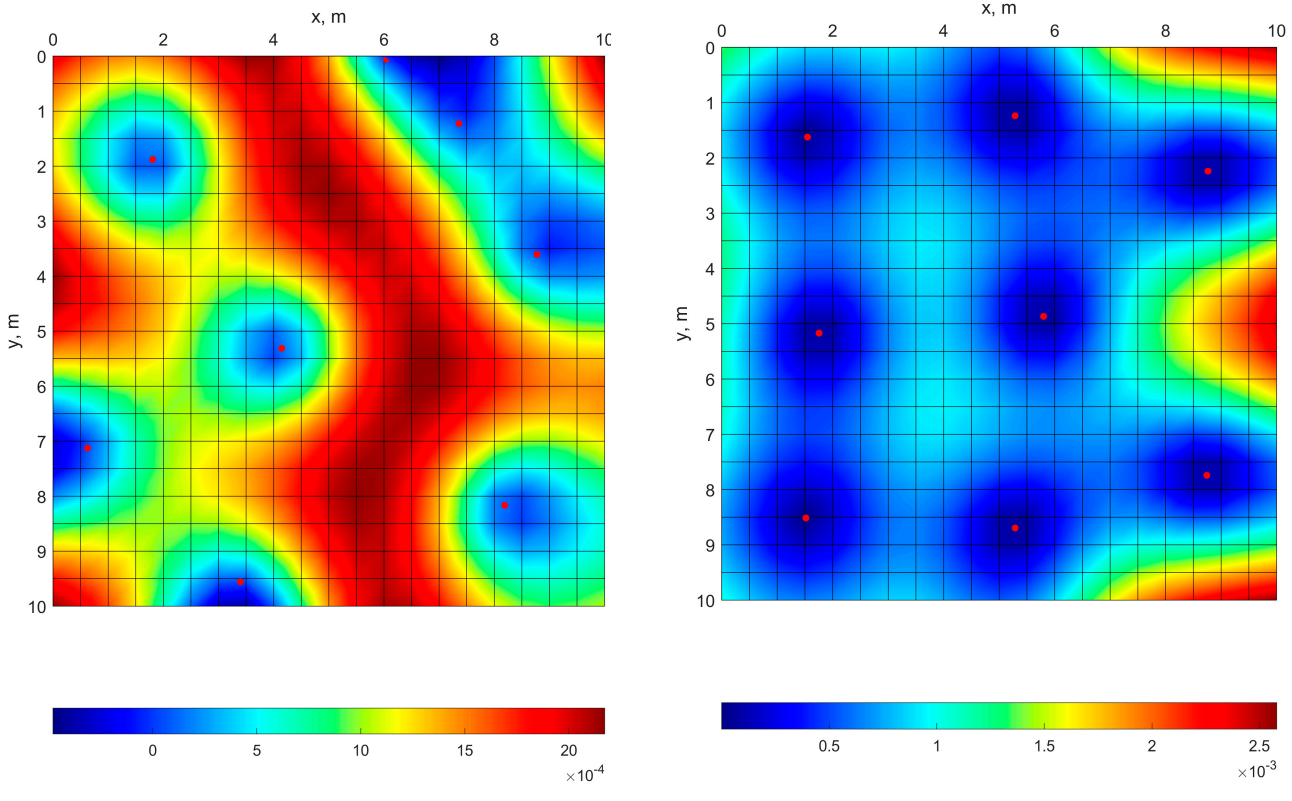

(**a**) (**b**)

Figure 10. Optimal location of the columns and isofields of vertical displacements (m) at $n = 8$: (**a**) from the minimum deflection condition; (**b**) from the PSE minimum condition.

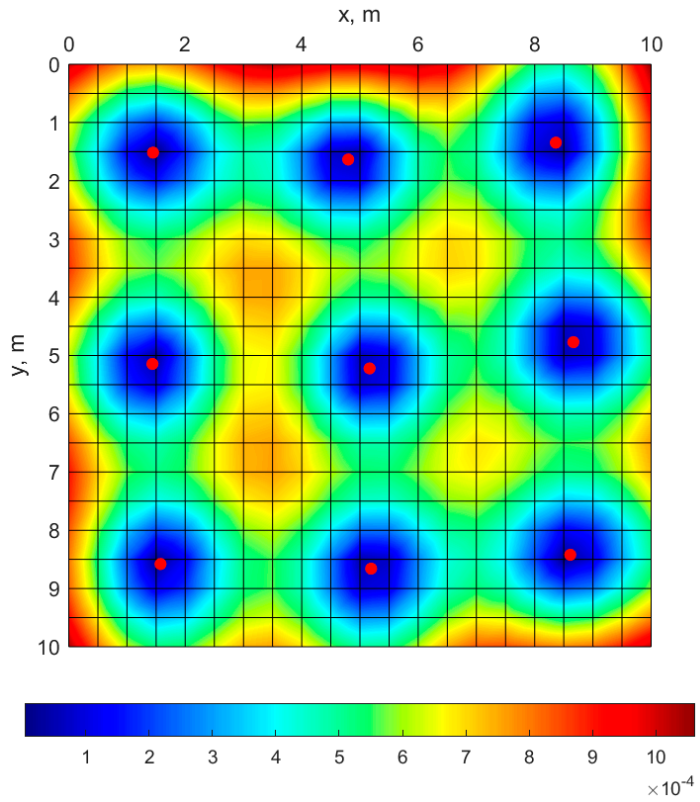

Figure 11. Optimal column arrangement at n = 9 from the minimum PSE condition, also providing minimum deflection.

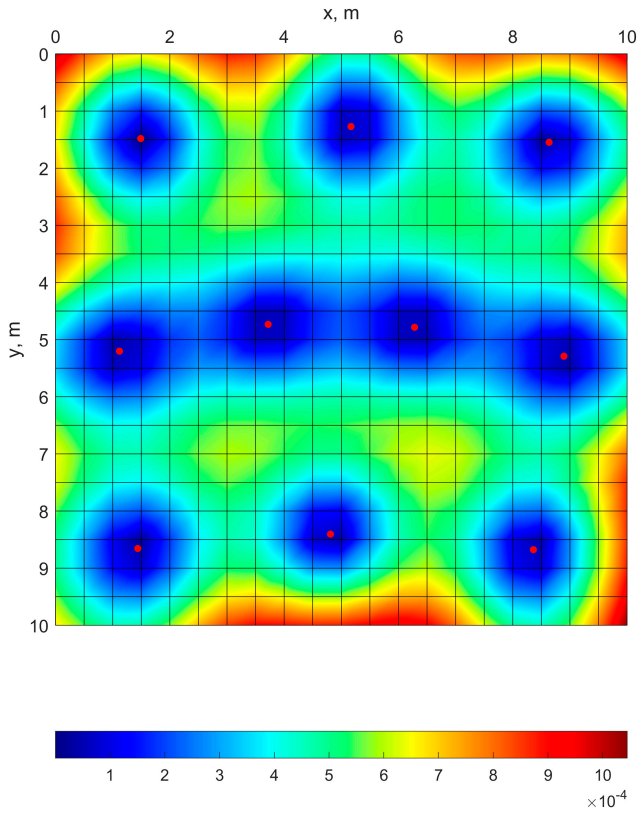

Figure 12. Optimal column arrangement at n = 10 from the minimum PSE condition, also providing minimum deflection.

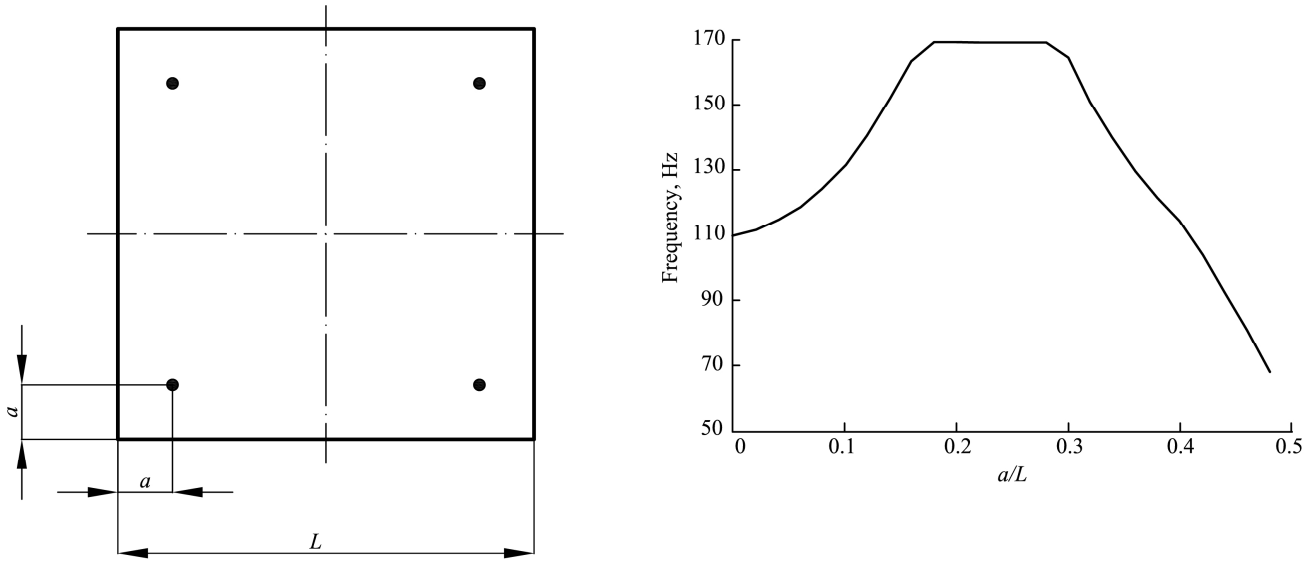

Figure 13. Dependence of the first frequency on the ratio *a*/*L* obtained in [29].

In the second stage, the developed technique was tested on the real object. The object of optimization was the beamless monolithic reinforced concrete floor slab of the scientific and laboratory complex building, the construction of which is planned in the city of Rostov-on-Don, Russia. The building under consideration consists of two parts separated by an expansion joint. The optimization of the supports position under the floor slab for each part was carried out separately. This article will present the results for the part of the building located to the right of the expansion joint. A schematic representation of the floor slab with columns and stiffening diaphragms is shown in Figure 14. Supports whose position remains unchanged are highlighted in black, and supports whose position may vary are highlighted in red. The supports along the outer contour of the building were assumed to be stationary to ensure the fastening of standard size facade panels. The position of the stiffening diaphragms was also assumed unchanged. The total number of columns, the position of which can vary, was equal to 7. The only accepted constraints were that the columns should not be outside the slab.

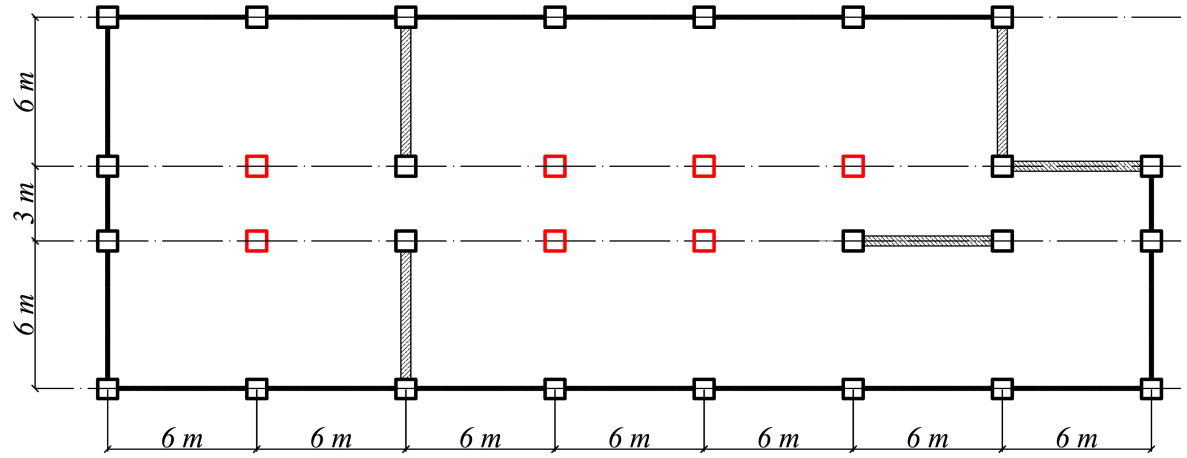

Figure 14. Scheme of the optimized floor slab.

The load on the slab was assumed to be uniformly distributed over the area with intensity q = 20 kN/m^2. The modulus of the elasticity of concrete was assumed to be 3×10^4 MPa; the thickness of the slab was 0.2 m. For the finite element discretization of the slab, triangular finite elements with a maximum side size 0.6 m were used. Figure 15 shows

isofields of vertical displacements with the initial arrangement of columns. The maximum deflection in the initial approximation was w_{max} = 19.3 mm, and the potential strain energy was W = 43.01 kJ.

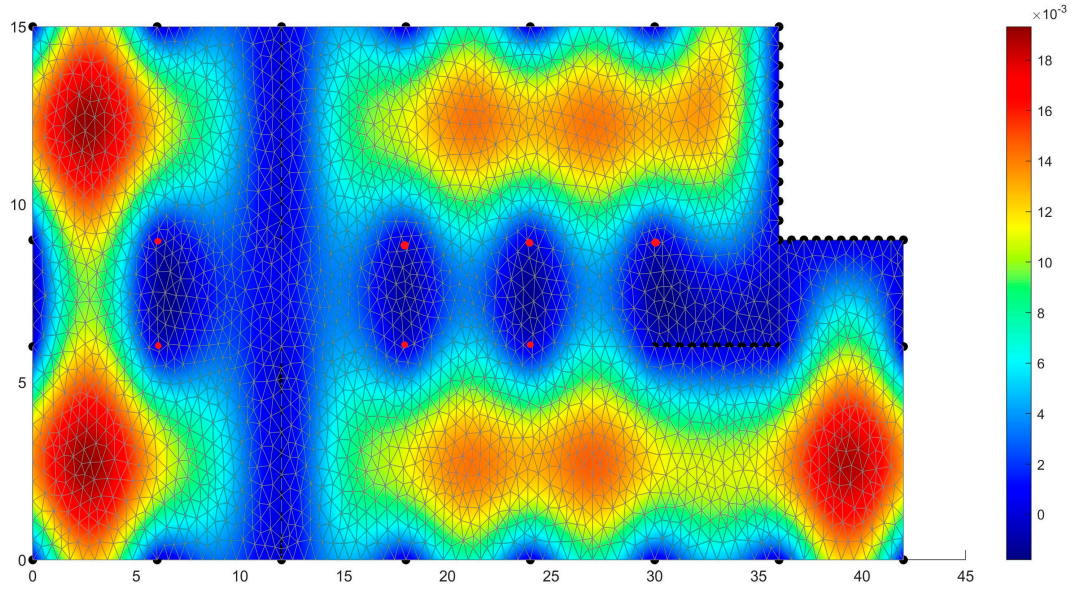

Figure 15. Isofields of vertical displacements (m) at the initial arrangement of columns.

When searching for the optimal location of supports based on the criterion of minimum deflection, the best result was obtained using the particle swarm algorithm. The optimal location of supports from the condition of minimum deflection along with the isofields of vertical displacements is shown in Figure 16. As a result of optimization, the maximum deflection decreased by 1.6 times from 19.3 to 12.1 mm. The potential strain energy also noticeably decreased from 43.01 kJ to 33.4 kJ.

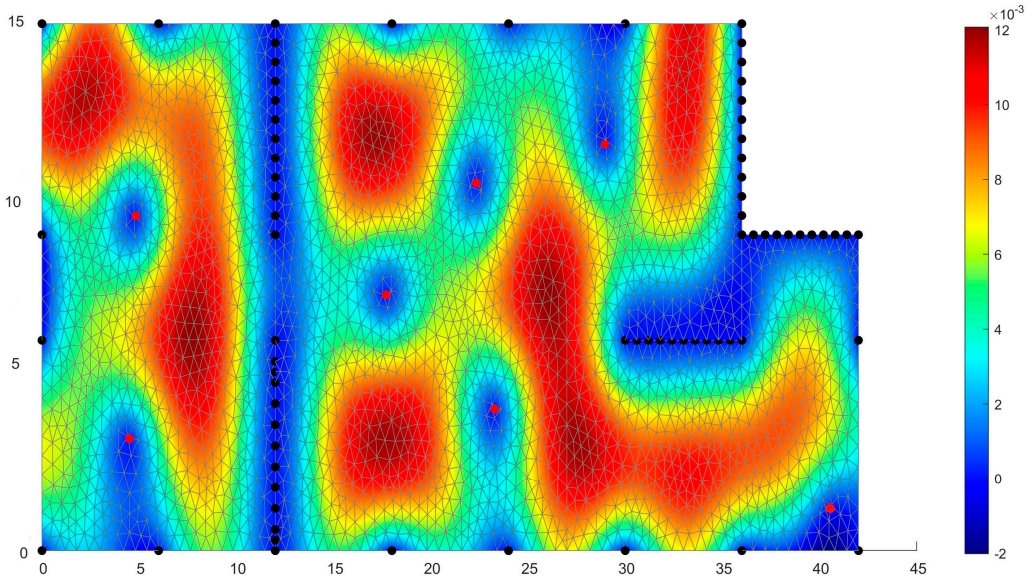

Figure 16. Optimal location of supports based on the condition of minimum deflection and the corresponding isofields of vertical displacements (m).

When optimizing according to the criterion of minimum potential strain energy, the best result was achieved using a genetic algorithm. Compared to the initial supports' location, the potential strain energy decreased by almost 1.5 times to 29.1 kJ. At the same

time, the maximum deflection remained almost unchanged and amounted to 18.8 mm. The optimal location of supports from the condition of minimum potential strain energy, as well as the corresponding isofields of deflections, are shown in Figure 17.

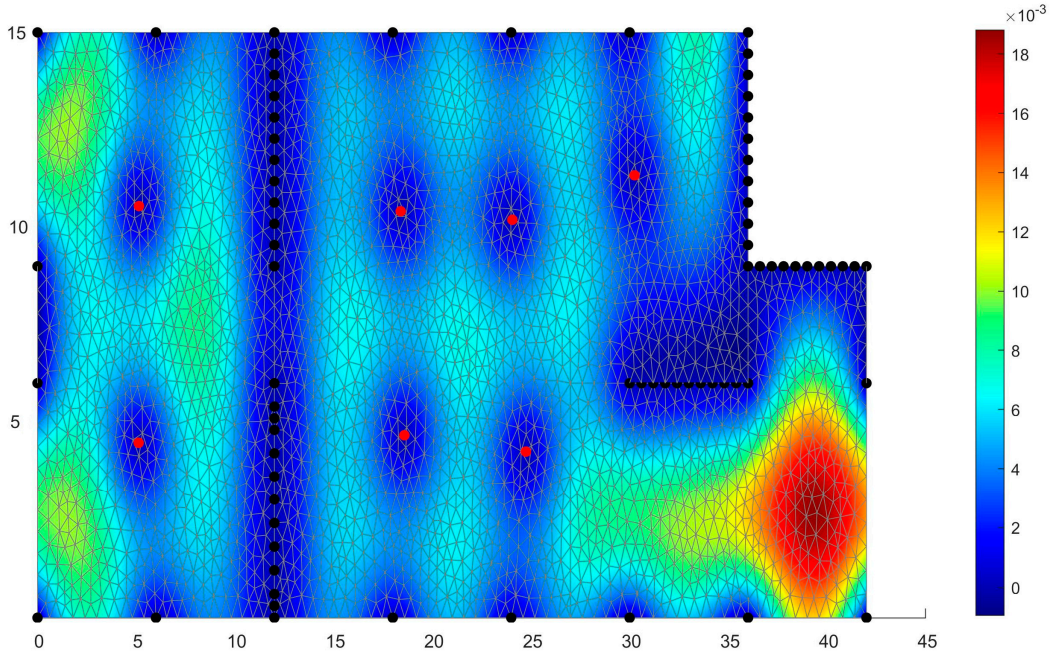

Figure 17. Optimal location of supports based on the condition of minimum potential strain energy and the corresponding isofields of vertical displacements (m).

4. Conclusions

A technique has been developed for determining the optimal location of point supports under a monolithic floor slab from the condition of minimum deflection and potential strain energy based on the finite element method in combination with nonlinear optimization methods. The proposed technique is implemented as the program in the MATLAB environment and allows one to optimize slabs of arbitrary configuration under arbitrary load. The finite element method algorithm is implemented in such a way that the position of the columns may not necessarily coincide with the nodes of the finite element mesh of the slab. This allows one to avoid re-generating the FE mesh when the position of the columns changes during the optimization process. Since the finite element mesh remains unchanged during the optimization process, at each iteration, there is no need to re-calculate the slab stiffness matrix, which leads to significant savings in computer time for solving the optimization problem.

The efficiency of six nonlinear optimization methods was compared using the example of a square slab in plan. It has been established that the particle swarm method and the genetic algorithm have the best efficiency for the considered problem. For solutions obtained using the pattern search method, simulated annealing method and internal point method, the maximum deflections are at least 1.2 times higher than for solutions obtained using the particle swarm method and genetic algorithm. It was shown that, in comparison with the criterion of minimum deflection, the criterion of minimum potential strain energy leads to solutions with greater symmetry and regularity. It has also been established that the results obtained from the condition of minimum potential strain energy for a square slab are close to the analytical solutions from the condition of the maximum of the first frequency.

The developed optimization technique was tested on the real object, which was the reinforced concrete monolithic floor slab of the scientific and laboratory complex. By varying the position of seven columns while maintaining the same position of the remaining columns and stiffening diaphragms, it was possible to reduce the maximum deflection by

1.6 times compared to the initial supports' location. When optimizing according to the criterion of minimum potential strain energy, it was possible to reduce it by 1.5 times.

The prospect of our further research will be the development of methods for optimizing monolithic floor slabs according to the criterion of cost, taking into account the fulfillment of the conditions of strength and rigidity. Also, the prospects for further research may include taking into account the influence of variable reinforcement on the optimal arrangement of columns, taking into account physical nonlinearity, as well as taking into account transverse shear deformations.

Author Contributions: Conceptualization, A.C. and V.A.; methodology, A.C.; software, V.T.; validation, A.C. and V.A.; formal analysis, A.C.; investigation, A.C.; resources, V.A.; data curation, V.T.; writing—original draft preparation, A.C.; writing—review and editing, V.T.; visualization, A.C.; supervision, A.C.; project administration, A.C.; funding acquisition, A.C. All authors have read and agreed to the published version of the manuscript.

Funding: This research received no external funding.

Data Availability Statement: The study did not generate any new data.

Acknowledgments: The authors would like to acknowledge the administration of Don State Technical University for their resources and financial support.

Conflicts of Interest: The authors declare no conflicts of interest. The funders had no role in the design of the study; in the collection, analyses, or interpretation of data; in the writing of the manuscript; or in the decision to publish the results.

References

1. Ahmadkhanlou, F.; Adeli, H. Optimum cost design of reinforced concrete slabs using neural dynamics model. *Eng. Appl. Artif. Intell.* **2005**, *18*, 65–72. [CrossRef]
2. Alcalá, J.; González-Vidosa, F.; Yepes, V.; Martí, J.V. Embodied energy optimization of prestressed concrete slab bridge decks. *Technologies* **2018**, *6*, 43. [CrossRef]
3. Aldwaik, M.; Adeli, H. Cost optimization of reinforced concrete flat slabs of arbitrary configuration in irregular highrise building structures. *Struct. Multidiscip. Optim.* **2016**, *54*, 151–164. [CrossRef]
4. Fraile-Garcia, E.; Ferreiro-Cabello, J.; Martinez-Camara, E.; Jimenez-Macias, E. Optimization based on life cycle analysis for reinforced concrete structures with one-way slabs. *Eng. Struct.* **2016**, *109*, 126–138. [CrossRef]
5. Mohammed, A.H.; Tayşi, N.; Nassani, D.E.; Hussein, A.K. Finite element analysis and optimization of bonded post-tensioned concrete slabs. *Cogent Eng.* **2017**, *4*, 1341288. [CrossRef]
6. Vatin, N.I.; Ivanov, A.Y.; Rutman, Y.L.; Chernogorskiy, S.A. Earthquake engineering optimization of structures by economic criterion. *Mag. Civ. Eng.* **2017**, *8*, 67–83. [CrossRef]
7. Yepes, V.; Martí Albiñana, J.V.; García-Segura, T. Design optimization of precast-prestressed concrete road bridges with steel fiber-reinforcement by a hybrid evolutionary algorithm. *Int. J. Comput. Methods Exp. Meas.* **2017**, *5*, 179–189. [CrossRef]
8. Zelickman, Y.; Amir, O. Optimization of post-tensioned concrete slabs for minimum cost. *Eng. Struct.* **2022**, *259*, 114132. [CrossRef]
9. Huber, T.; Burger, J.; Mata-Falcón, J.; Kaufmann, W. Structural design and testing of material optimized ribbed RC slabs with 3D printed formwork. *Struct. Concr.* **2023**, *24*, 1932–1955. [CrossRef]
10. Moita, J.S.; Araújo, A.L.; Correia, V.F.; Soares, C.M.M.; Herskovits, J. Material distribution and sizing optimization of functionally graded plate-shell structures. *Compos. Part B Eng.* **2018**, *142*, 263–272. [CrossRef]
11. Andreev, V.I.; Barmenkova, E.V.; Potekhin, I.A. Way of optimization of stress state of elements of concrete structures. *Procedia Eng.* **2016**, *153*, 37–44. [CrossRef]
12. Andreev, V.I. About one way of optimization of the thick-walled shells. *Appl. Mech. Mater.* **2012**, *166*, 354–358. [CrossRef]
13. Andreev, V.I. Optimization of thick-walled shells based on solutions of inverse problems of the elastic theory for inhomogeneous bodies. In *Computer Aided Optimum Design in Engineering*; WIT Press: Billerica MA, USA, 2012; pp. 189–202.
14. Andreev, V.I.; Chepurnenko, A.S.; Jazyev, B.M. Model of equal-stressed cylinder based on the Mohr failure criterion. *Adv. Mater. Res.* **2014**, *887*, 869–872. [CrossRef]
15. Yazyev, S.; Bekkiev, M.; Peresypkin, E.; Turko, M. Task for a Prestressed Reinforced Concrete Cylinder with External Reinforcement and Cylinder Optimization by Varying the Modulus of Elasticity. In Proceedings of the Energy Management of Municipal Transportation Facilities and Transport, Khabarovsk, Russia, 10–13 April 2017; pp. 869–876. [CrossRef]
16. Beskopylny, A.; Stel'makh, S.A.; Shcherban, E.M.; Mailyan, L.R.; Meskhi, B. Nano modifying additive micro silica influence on integral and differential characteristics of vibrocentrifuged concrete. *J. Build. Eng.* **2022**, *51*, 104235. [CrossRef]

17. Beskopylny, A.N.; Stel'makh, S.A.; Shcherban', E.M.; Mailyan, L.R.; Meskhi, B.; Beskopylny, N.; El'shaeva, D. Influence of the Chemical Activation of Aggregates on the Properties of Lightweight Vibro-Centrifuged Fiber-Reinforced Concrete. *J. Compos. Sci.* **2022**, *6*, 273. [CrossRef]
18. Beskopylny, A.N.; Shcherban', E.M.; Stel'makh, S.A.; Mailyan, L.R.; Meskhi, B.; Evtushenko, A.; Beskopylny, N. Nano-Modified Vibrocentrifuged Concrete with Granulated Blast Slag: The Relationship between Mechanical Properties and Micro-Structural Analysis. *Materials* **2022**, *15*, 4254. [CrossRef] [PubMed]
19. Shcherban', E.M.; Stel'makh, S.A.; Beskopylny, A.; Mailyan, L.R.; Meskhi, B. Influence of Mechanochemical Activation of Concrete Components on the Properties of Vibro-Centrifugated Heavy Concrete. *Appl. Sci.* **2021**, *11*, 10647. [CrossRef]
20. Stel'makh, S.A.; Shcherban', E.M.; Beskopylny, A.N.; Mailyan, L.R.; Meskhi, B.; Butko, D.; Smolyanichenko, A.S. Influence of Composition and Technological Factors on Variatropic Efficiency and Constructive Quality Coefficients of Lightweight Vibro-Centrifuged Concrete with Alkalized Mixing Water. *Appl. Sci.* **2021**, *11*, 9293. [CrossRef]
21. Chepurnenko, A.; Efimenko, E.; Mailyan, D.; Yazyev, B. The location of supports under the monolithic reinforced concrete slabs optimization. *Mag. Civ. Eng.* **2021**, *4*, 10404. [CrossRef]
22. Lai, M.; Zucca, M.; Meloni, D.; Reccia, E.; Cazzani, A. Thin corrugated-edge shells inspired by Nervi's dome: Numerical insight about their mechanical behaviour. *Thin-Walled Struct.* **2023**, *191*, 111076. [CrossRef]
23. Aydin, E.; Dutkiewicz, M.; Öztürk, B.; Sonmez, M. Optimization of elastic spring supports for cantilever beams. *Struct. Multidiscip. Optim.* **2020**, *62*, 55–81. [CrossRef]
24. Hauser, B.R.; Wang, B.P. Optimal design of a parallel beam system with elastic supports to minimize flexural response to harmonic loading using a combined optimization algorithm. *Struct. Multidiscip. Optim.* **2018**, *58*, 1453–1465. [CrossRef]
25. Kozikowska, A. Multi-objective topology and geometry optimization of statically determinate beams. *Struct. Eng. Mech. Int'l J.* **2019**, *70*, 367–380.
26. Wang, B.P.; Chen, J.L. Application of genetic algorithm for the support location optimization of beams. *Comput. Struct.* **1996**, *58*, 797–800. [CrossRef]
27. Xie, C.N.; Li, X.F. Optimal location of ring support for heavy Mindlin plates under axisymmetric loading. *Proc. Inst. Mech. Eng. Part C J. Mech. Eng. Sci.* **2018**, *232*, 1270–1279. [CrossRef]
28. Won, K.M.; Park, Y.S. Optimal support positions for a structure to maximize its fundamental natural frequency. *J. Sound Vib.* **1998**, *213*, 801–812. [CrossRef]
29. Wang, D.; Jiang, J.S.; Zhang, W.H. Optimization of support positions to maximize the fundamental frequency of structures. *Int. J. Numer. Methods Eng.* **2004**, *61*, 1584–1602. [CrossRef]
30. Wang, D. Optimization of support positions to minimize the maximal deflection of structures. *Int. J. Solids Struct.* **2004**, *41*, 7445–7458. [CrossRef]
31. Wang, D. Optimal design of structural support positions for minimizing maximal bending moment. *Finite Elem. Anal. Des.* **2006**, *43*, 95–102. [CrossRef]
32. Wang, C.M.; Wang, L.; Ang, K.K.; Liew, K.M. Optimization of internal line support positions for plates against vibration. *J. Struct. Mech.* **1993**, *21*, 429–454. [CrossRef]
33. Wang, D.; Friswell, M.I. Support position optimization with minimum stiffness for plate structures including support mass. *J. Sound Vib.* **2021**, *499*, 116003. [CrossRef]
34. Jihong, Z.; Weihong, Z. Maximization of structural natural frequency with optimal support layout. *Struct. Multidiscip. Optim.* **2006**, *31*, 462–469. [CrossRef]
35. Aydın, E.; Öztürk, B.A.K.İ.; Dutkiewicz, M. Determination of optimal elastic springs for cantilever beams supported by elastic foundation. In Proceedings of the Engineering Mechanics 2018, Svratka, Czech Republic, 14–17 May 2018; pp. 33–36. [CrossRef]
36. Wang, D.; Wen, M. Vibration attenuation of beam structure with intermediate support under harmonic excitation. *J. Sound Vib.* **2022**, *532*, 117008. [CrossRef]
37. Kitov, Y.; Verevicheva, M.; Vatulia, G.; Orel, Y.; Deryzemlia, S. Design solutions for structures with optimal internal stress distribution. *MATEC Web Conf.* **2017**, *133*, 03001. [CrossRef]
38. Loureiro, D.; Loja, M.A.; Silva, T.A. Optimal location of supports in beam structures using genetic algorithms. In Proceedings of the 2014 Sixth World Congress on Nature and Biologically Inspired Computing, Porto, Portugal, 30 July–1 August 2014; pp. 293–298. [CrossRef]
39. Jang, G.W.; Shim, H.S.; Kim, Y.Y. Optimization of support locations of beam and plate structures under self-weight by using a sprung structure model. *J. Mech. Des.* **2009**, *131*, 021005. [CrossRef]
40. Akhtyamova, L. Optimization of a truncated conical shell wind turbine tower. *Constr. Archit.* **2021**, *9*, 51–55. [CrossRef]
41. Efimenko, E.A.; Chepurnenko, A.S.; Mailyan, D.R.; Saibel, A.V. The industrial buildings reinforced concrete floor slabs with rational choice of the column pitch. *IOP Conf. Ser. Mater. Sci. Eng.* **2020**, *896*, 012004. [CrossRef]
42. Zienkiewicz, O.C.; Taylor, R.L. *The Finite Element Method for Solid and Structural Mechanics*; Butterworth-Heinemann: Oxford, UK, 2005.
43. Bathe, K.J. *Finite Element Method*; Wiley: New York, NY, USA, 2007.
44. Belhocine, A.; Shinde, D.; Patil, R. Thermo-mechanical coupled analysis based design of ventilated brake disc using genetic algorithm and particle swarm optimization. *JMST Adv.* **2021**, *3*, 41–54. [CrossRef]

45. Murlidhar, B.R.; Sinha, R.K.; Mohamad, E.T.; Sonkar, R.; Khorami, M. The effects of particle swarm optimisation and genetic algorithm on ANN results in predicting pile bearing capacity. *Int. J. Hydromechatron.* **2020**, *3*, 69–87. [CrossRef]
46. Novoselov, O.G.; Sabitov, L.S.; Sibgatullin, K.E.; Sibgatullin, E.S.; Klyuev, A.S.; Klyuev, S.V.; Shorstova, E.S. Method for calculating the strength of massive structural elements in the general case of their stress-strain state (kinematic method). *Constr. Mater. Prod.* **2023**, *6*, 5–17. [CrossRef]
47. Novoselov, O.G.; Sabitov, L.S.; Sibgatullin, K.E.; Sibgatullin, E.S.; Klyuev, A.V.; Klyuev, S.V.; Shorstova, E.S. Method for calculating the strength of massive structural elements in the general case of their stress-strain state (parametric equations of the strength surface). *Constr. Mater. Prod.* **2023**, *6*, 104–120. [CrossRef]
48. Jiao, J.; Ghoreishi, S.M.; Moradi, Z.; Oslub, K. Coupled particle swarm optimization method with genetic algorithm for the static–dynamic performance of the magneto-electro-elastic nanosystem. *Eng. Comput.* **2021**, *38*, 1–15. [CrossRef]
49. Dziwiński, P.; Bartczuk, Ł. A new hybrid particle swarm optimization and genetic algorithm method controlled by fuzzy logic. *IEEE Trans. Fuzzy Syst.* **2019**, *28*, 1140–1154. [CrossRef]
50. Moslehi, F.; Haeri, A. A novel hybrid wrapper–filter approach based on genetic algorithm, particle swarm optimization for feature subset selection. *J. Ambient Intell. Humaniz. Comput.* **2020**, *11*, 1105–1127. [CrossRef]
51. Memon, M.A.; Siddique, M.D.; Mekhilef, S.; Mubin, M. Asynchronous particle swarm optimization-genetic algorithm (APSO-GA) based selective harmonic elimination in a cascaded H-bridge multilevel inverter. *IEEE Trans. Ind. Electron.* **2021**, *69*, 1477–1487. [CrossRef]
52. Omidinasab, F.; Goodarzimehr, V. A hybrid particle swarm optimization and genetic algorithm for truss structures with discrete variables. *J. Appl. Comput. Mech.* **2020**, *6*, 593–604. [CrossRef]
53. Son, J.H.; Kwak, B.M. Optimization of boundary conditions for maximum fundamental frequency of vibrating structures. *AIAA J.* **1993**, *31*, 2351–2357. [CrossRef]